



Cite this: *J. Mater. Chem. B*, 2018, 6, 3946

## Regenerable smart antibacterial surfaces: full removal of killed bacteria *via* a sequential degradable layer†

Yangcui Qu,<sup>‡a</sup> Ting Wei,<sup>‡a</sup> Jian Zhao,<sup>‡b</sup> Shuaibing Jiang,<sup>a</sup> Peng Yang,<sup>id \*b</sup> Qian Yu,<sup>id \*a</sup> and Hong Chen,<sup>id a</sup>

Conventional antibacterial surfaces are becoming less effective due to the emergence of multidrug resistant bacteria; in addition, difficulties related to the accumulation of killed bacteria are generally encountered. To circumvent these problems, in the present work, an antibiotic-free and regenerable antibacterial hybrid film with both photothermal bactericidal activity and bacteria-releasing properties was fabricated on diverse substrates by sequential deposition of a gold nanoparticle layer (GNPL) and a phase-transitioned lysozyme film (PTLF). Due to the photothermal effect of the GNPL, the hybrid film was able to kill >99% of attached bacteria under near-infrared laser irradiation in 5 min. Moreover, the topmost PTLF layer could be degraded and detached from the surface by immersion in vitamin C solution for a short period, leading to removal of the killed bacteria and surface regeneration. The surface could be used and regenerated in this way through multiple cycles for long-term effective performance. The surface fabrication process is simple and environmentally friendly, and can be applied to diverse materials. These hybrid films thus offer a viable alternative for the killing and removal of adherent bacteria (particularly multidrug resistant bacteria) on the surfaces of medical devices for *in vitro* applications.

Received 28th April 2018,  
Accepted 17th May 2018

DOI: 10.1039/c8tb01122b

rsc.li/materials-b

### 1. Introduction

Attachment and subsequent colonization by bacteria on the surfaces of synthetic materials and devices pose serious problems in both human healthcare and industrial applications.<sup>1,2</sup> Therefore, antibacterial surfaces with capability to prevent bacterial attachment and biofilm formation have been a long-standing focus of research.<sup>3–5</sup> Conventional antibacterial surfaces

usually rely on natural or synthetic antibiotics or other biocidal compounds;<sup>6–10</sup> however, these surfaces are becoming less effective due to the emergence of multidrug resistant (MDR) bacteria, which have proved to be especially problematic in both hospital and community settings.<sup>11,12</sup> Therefore, alternative antibiotic-free antibacterial surfaces that can kill adherent bacteria irrespective of their antibiotic susceptibility are urgently needed.

Photothermal therapy using strong light absorbers to generate local heat for physical destruction of bacteria provides a promising approach for circumventing the problem of antibiotic resistance.<sup>13–15</sup> In particular, near infrared (NIR) irradiation in the range of 700–1100 nm is most attractive for photothermal therapy because of its ability to penetrate biological tissues with sufficient intensity and with minimal tissue damage.<sup>16</sup> In recent years, there has been considerable interest in NIR photothermal materials such as gold-based nanomaterials,<sup>17–20</sup> reduced graphene oxide (rGO),<sup>21–23</sup> and polypyrrole nanoparticles<sup>24</sup> for antibacterial applications. Among these materials, gold-based nanoparticles (GNPs) hold great promise as bactericidal agents because of their highly efficient light-to-heat conversion capability *via* surface plasmon resonance in the NIR region, their relatively good biocompatibility, and their great potential for functionalization with bacterial affinity ligands.<sup>25,26</sup> Several GNP-based photothermal bactericides have been developed against bacteria in suspension

<sup>a</sup> State and Local Joint Engineering Laboratory for Novel Functional Polymeric Materials, College of Chemistry, Chemical Engineering and Materials Science, Soochow University, 199 Ren'ai Road, Suzhou, 215123, P. R. China. E-mail: yuqian@suda.edu.cn

<sup>b</sup> Key Laboratory of Applied Surface and Colloids Chemistry, Ministry of Education, School of Chemistry and Chemical Engineering, Shaanxi Normal University, Xi'an, 710119, China. E-mail: yangpeng@snnu.edu.cn

† Electronic supplementary information (ESI) available: Materials and methods, statistical analysis, surface morphology, surface elemental compositions, photothermal properties, bactericidal activity evaluated *via* live/dead staining assay, Vc-induced degradation of PTLF, bactericidal activity evaluated *via* colony counting assay, antibacterial performance of the GNPL-PTLF surface against a MDR bacterial strain, Vc-triggered bacteria-releasing abilities of the GNPL-PTLF surface, sequential degradation of PTLF, storage stability and long-term effectiveness of the GNPL-PTLF surface, and surface properties and antibacterial performances of GNPL and GNPL-PTLF surfaces on different substrates. See DOI: 10.1039/c8tb01122b

‡ These authors contributed equally.



**Scheme 1** Schematic illustration of a smart antibacterial surface based on a GNPL–PTLF hybrid film with photothermal bacteria-killing capability and Vc-triggered bacteria-releasing ability.

and the antibacterial efficacy and targeting ability of these bactericides could be further improved by conjugation with specific antibodies.<sup>27–29</sup> However, the use of GNPs as photothermal agents for surface modification to kill attached bacteria under NIR laser irradiation has not been reported.

Previous reports have suggested that photothermal antibacterial coatings based on immobilized other photothermal agents (such as polyaniline,<sup>30</sup> polydopamine,<sup>31</sup> or  $\text{Cs}_{0.33}\text{WO}_3$  nanoparticles<sup>32</sup>) that can destroy attached bacteria on surfaces under irradiation with NIR or solar light provide an alternative approach to combat infection and contamination on surfaces resulting from bacterial adhesion, particularly MDR bacteria. However, these coatings suffer from the same inherent drawbacks as traditional antibacterial surfaces based on contact-killing mechanisms, and even if they show high bactericidal efficiency, they remain contaminated by dead bacteria and other debris, which not only provide nutrients for subsequent bacterial interactions, but may also trigger severe immune responses and inflammation.<sup>33</sup> To circumvent the problem of dead bacteria, a promising “kill-and-release” strategy has been proposed for the development of smart antibacterial surfaces with the capability of not only killing the attached bacteria but also releasing dead bacteria and debris “on demand” under an appropriate stimulus.<sup>34,35</sup> Compared with conventional bactericidal surfaces, such smart surfaces provide a more promising solution for the prevention of initial bacterial attachment and subsequent biofilm formation. In particular, the triggered-cleaning properties and repeatable function switching make these surfaces more suitable for applications where long-term antibacterial activity is required.<sup>36–42</sup> However, to the best of our knowledge, smart photothermal antibacterial surfaces with bacteria-releasing properties are yet to be developed.

In the work reported herein, we have developed an efficient smart antibacterial hybrid coating with both photothermal bactericidal activity and bacteria-releasing properties as illustrated in Scheme 1. This hybrid coating is composed of two functional layers. The first is a gold nanoparticle layer (GNPL) composed of GNP aggregates which serve as the photothermal bactericidal agent. Compared with dispersed GNPs, the aggregated GNPs exhibit a more efficient photothermal effect due to the red-shifted absorption.<sup>43</sup> In addition, the GNPL possesses a unique micro-nanotopography that provides multiple sites for contact with bacteria and facilitates local hyperthermia induced by NIR laser irradiation. We showed previously that the GNPL can be used as an efficient photoporation platform for intracellular

delivery of macromolecules to mammalian cells under NIR laser irradiation.<sup>44,45</sup> Based on the same principle, it is anticipated that the GNPL can also be used as an effective antibacterial material on which attached bacteria can be destroyed photothermally. In addition, the GNPL was coated with a thin phase-transitioned lysozyme film (PTLF) as a contamination releasing layer. PTLF was recently developed in our previous works as a novel biocompatible two-dimensional (2D) proteinaceous nanofilm with versatile applications in tissue engineering,<sup>46</sup> antimicrobial materials,<sup>47</sup> surface functionalization and biomimetic adhesive bonding to virtually any substrate.<sup>48–51</sup> For substrates immersed in phase-transitioned lysozyme solution, a PTLF composed of densely aggregated oligomers within amyloid-like structures was shown to form on the surface in a few minutes. Such PTLFs are transparent and exhibit strong substrate bonding even in extreme pH conditions or under gas plasma treatment.<sup>52,53</sup> It is thus expected that the addition of PTLF will not affect the light-to-heat conversion capability of the GNPL or the bactericidal efficacy of the GNPL. As an alternative, we showed in the present work that the degradation of PTLF can be triggered in a closely controlled manner by treatment with vitamin C (Vc). Almost all of the killed bacteria could be removed by incubating the surface in Vc solution for a short time period (10 min) due to the degradation of the topmost layer of PTLF. The GNPL and PTLF are relatively simple, environmentally friendly materials, and can be applied to diverse substrates. In addition, the GNPL–PTLF coating can be used repeatedly over multiple “kill-and-release” cycles, which is of particular importance for long-term usage.

## 2. Results and discussion

### 2.1. Surface preparation and characterization

Fabrication of the GNPL–PTLF hybrid surface involved sequential deposition of GNPL and PTLF on a substrate. A stable GNPL was prepared on a gold substrate *via* a chemical plating method as reported previously.<sup>54</sup> As observed by scanning electron microscopy (SEM), the GNPL was composed of numerous aggregates of GNPs uniformly distributed on the surface (Fig. 1). The density of these aggregates and the corresponding surface roughness of the GNPL could be further adjusted by changing the quantity of plating solution used for preparation (Fig. S1, ESI†). Afterwards, a thin PTLF was formed directly on the GNPL by immersing in a phase transitioned lysozyme buffer for 2 h.<sup>47</sup> As control, a smooth

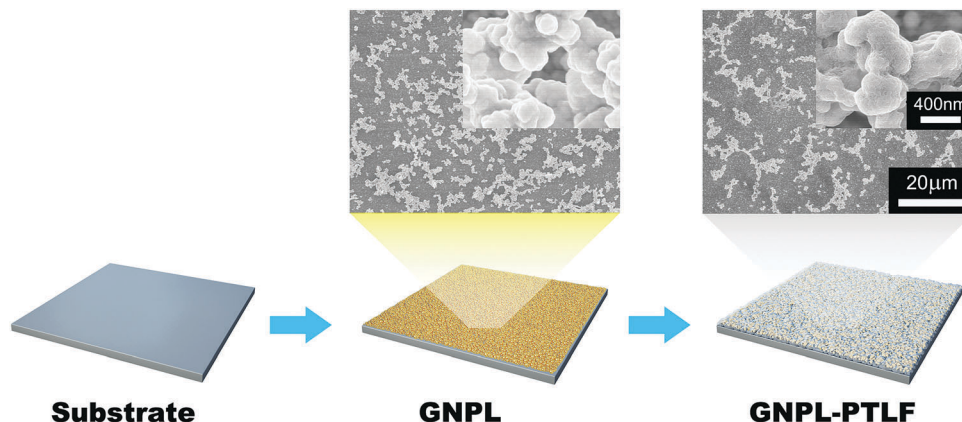


Fig. 1 Schematic depicting the procedure for preparation of GNPL-PTLF on a substrate. The surface morphology of the GNPL surface before and after coating with PTLF was observed using SEM.

gold surface coated with PTLF (Au-PTLF) was prepared in a similar way. It is noted that the entire preparation process was conducted in aqueous solution in a simple and environmentally friendly manner. For a “single” typical coating process, the thickness of the PTLF was  $54.8 \pm 1.6$  nm as measured by ellipsometry; this could be increased by additional coating steps. The PTLF was continuous and gap-free; no large aggregates were observed and the gold and GNPL surfaces were completely covered as observed by SEM (Fig. 1 and Fig. S2, ESI<sup>†</sup>). No color change was seen after formation of the PTLF, indicating excellent optical transparency. The integration of the PTLF led to a significant increase in surface hydrophobicity such that the water contact angle increased from  $43.8 \pm 9.7^\circ$  (pristine GNPL surface) to  $98.7 \pm 3.6^\circ$  (GNPL-PTLF surface), possibly due to synergy between surface chemistry and topography.<sup>55</sup> The successful formation of the PTLF on the GNPL was confirmed by X-ray photoelectron spectroscopy (XPS) where the gold signal decreased and the nitrogen signal increased, reflecting the presence of a proteinaceous substrate (Table S1, ESI<sup>†</sup>).

Previous work demonstrated that aggregated GNPs converted absorbed NIR laser irradiation to heat more efficiently than dispersed GNPs, and that the GNPL exhibited excellent photothermal properties upon NIR laser irradiation.<sup>44</sup> In the present work, the photothermal effects of the films were evaluated by monitoring the surface temperature during exposure to an 808 nm continuous-wave (CW) laser at  $2.3 \text{ W cm}^{-2}$  in the dry state *in situ* using an infrared thermal camera. As shown in Fig. 2a, under laser irradiation for 90 s, the surface temperature of the GNPL increased rapidly to  $130^\circ\text{C}$ ; both the rate of temperature increase and the final temperature on the GNPL were much higher than on the control Au surface due to the localized surface plasmon resonance (LSPR) of the GNP aggregates.<sup>56</sup> Moreover, the presence of the PTLF on the GNPL did not influence the light-to-heat conversion efficiency because of the high transparency of the PTLF allowing  $\sim 100\%$  NIR transmission.<sup>52</sup>

It has been demonstrated that elevated temperatures may cause irreversible cell damage *via* disruption of metabolic signals, denaturation of proteins, and rupture of cell walls.<sup>14</sup> Therefore we proceeded to test the NIR-induced antibacterial activity of the GNPL-PTLF hybrid surfaces. Preliminary results

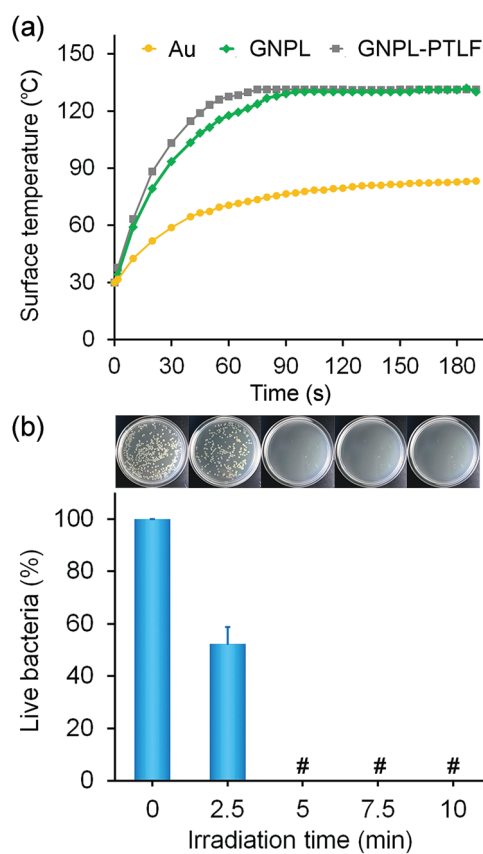


Fig. 2 (a) Comparison of photothermal properties of a smooth, unmodified gold surface, a GNPL surface and a GNPL-PTLF surface under NIR laser irradiation ( $2.3 \text{ W cm}^{-2}$ ) in the dry state. (b) Effect of irradiation time on the photothermal biocidal activity of the GNPL-PTLF surface against *E. coli* evaluated by colony-counting assay. # indicates live bacteria percent  $< 0.5$ . Error bars represent the standard deviation of the mean ( $n = 3$ ).

indicated that the photothermal bactericidal performance of the GNPL surface was influenced by the density of GNP aggregates, laser power density, and irradiation time: higher density of aggregates, higher laser power density, and longer irradiation time led to greater killing efficiency (Fig. S3–S5, ESI<sup>†</sup>

and Fig. 2b). The use of a GNPL optimized for aggregate density and a 5 min irradiation time led to the killing of >99.9% of attached bacteria; these conditions were therefore chosen for subsequent experiments.

After confirming the excellent photothermal bactericidal capability of the GNPL–PTLF hybrid film, we further tested its bacteria-releasing ability based on the stimulus-responsive degradation of the PTLF. In the formation of PTLF on the gold substrate, the protein unfolded upon treatment with the disulfide breaker tris(2-carboxyethyl)phosphine (TCEP); hydrophobic residues were thereby exposed to the solution. Hydrophobicity-induced aggregation of partially unfolded lysozyme chains then occurred, and a PTLF rich in  $\beta$ -sheet structures was formed on the substrate with robust interfacial adhesion.<sup>52</sup> For the degradation of the PTLF under mild conditions, we exploited the properties of vitamin C (Vc), a naturally occurring molecule with strong anti-oxidant activity. It is reported that Vc inhibits amyloid formation *in vitro* due to its bonding to the exposed hydrogen atoms of the N–H groups in the  $\beta$ -sheet backbone, which disrupts the hydrogen bonding between  $\beta$ -sheets that is necessary for the stabilization of amyloid structures.<sup>57</sup> Therefore, it was hypothesized that incubation of PTLF in Vc solution might degrade the topmost layer of the PTLF, *i.e.* the PTLF could be used as a “sacrificial layer” for removal of contaminants including dead bacteria.

To test this hypothesis, the effects of Vc solution concentration and incubation time on Vc-induced degradation of PTLF were systematically investigated (Fig. S6, ESI†). It was found that degradation increased with increasing concentration of Vc solution and increasing incubation time. Considering the degradation efficiency and potential cytotoxicity of Vc at high concentration, optimal degradation conditions were determined to be Vc = 100 mM and 10 min incubation time and were used in subsequent experiments. Under these conditions, the PTLF layer thickness on Au–PTLF decreased from  $54.8 \pm 1.6$  nm to  $9.7 \pm 1.1$  nm. The residual film may be due to strong Au–S bonding with degraded protein fragments containing thiol groups.<sup>52</sup> The partial degradation and detachment of PTLF from the GNPL surface under Vc treatment was confirmed by changes in surface wettability and elemental composition. As shown in Fig. 3b, the water contact angle of GNPL–PTLF did not change significantly

after Vc treatment, suggesting that the treated surface retained the properties of PTLF. In addition, as shown in Fig. 3c, the gold signal disappeared on attachment of PTLF to the GNPL. Upon immersion of the GNPL–PTLF surface in Vc solution, the gold content “recovered” to about half that of the GNPL, demonstrating the partial degradation of the PTLF.

## 2.2. Photothermal inactivation of bacteria

Antibacterial performance was evaluated using two common clinically relevant wound pathogens, Gram-positive *S. aureus* and Gram-negative *E. coli*, by a universally adopted colony-counting assay. Smooth Au, smooth Au–PTLF, and GNPL surfaces were used as controls. The surfaces were incubated in a suspension of *S. aureus* or *E. coli* ( $1 \times 10^7$  cells mL<sup>-1</sup>) at 37 °C for 1 h, followed by exposure to an 808 nm NIR laser for 5 min or being kept in the dark. Bacteria adherent on the surfaces were detached by sonication and the resulting bacterial suspensions were diluted to an appropriate concentration and plated in triplicate on Luria–Bertani (LB) agar plates. The plates were incubated at 37 °C for 24 h and the bacterial colonies formed were counted (typical visual images are shown in Fig. S7, ESI†). For each type of surface, the killing efficiency was calculated as the ratio of the number of colonies after and before NIR treatment. As shown in Fig. 4a, the Au and Au–PTLF surfaces showed negligible killing for both bacterial strains (efficiency <20%), indicating that NIR alone did not induce bactericidal activity. In contrast, the GNPL and GNPL–PTLF surfaces showed high killing efficiencies against both *E. coli* (>99%) and *S. aureus* (>96%) upon treatment with NIR laser irradiation. The slight difference in the killing efficiency between the two bacterial strains may be attributable to the difference in their sensitivity to heat (Gram-positive bacteria have greater heat resistance than Gram-negative bacteria).<sup>21,58</sup> To further investigate the killing mechanism, the surface morphologies of attached bacteria on Au and GNPL–PTLF surfaces with and without NIR laser treatment were observed using SEM. As shown in Fig. 4b, without laser treatment all of the bacteria on the Au and GNPL–PTLF surfaces exhibited intact and smooth surfaces and maintained their normal shapes (sphere-like for *S. aureus*, rod-like for *E. coli*). Exposure to NIR laser irradiation for 5 min did not affect the morphology of bacteria on

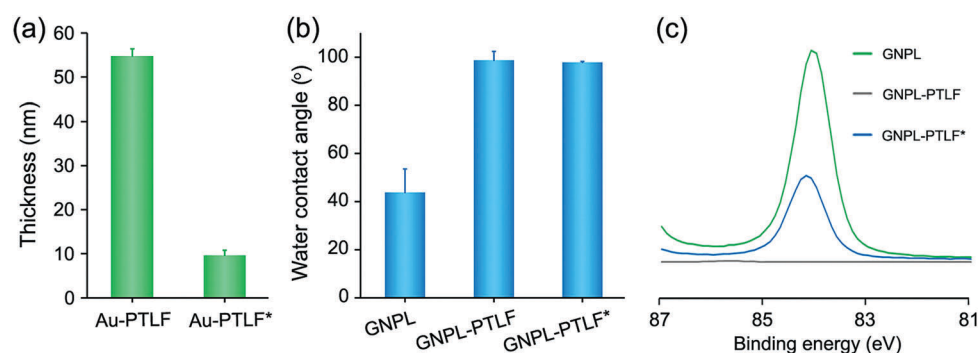


Fig. 3 (a) Thickness of Au–PTLF and Au–PTLF\* surfaces. (b) Water contact angle, and (c) high-resolution XPS Au<sub>4s</sub> spectra of GNPL, GNPL–PTLF and GNPL–PTLF\* surfaces. Au–PTLF\* and GNPL–PTLF\* represent Au–PTLF and GNPL–PTLF surfaces after incubation in 100 mM Vc solution for 10 min, respectively. Error bars represent the standard deviation of the mean ( $n = 6$ ).

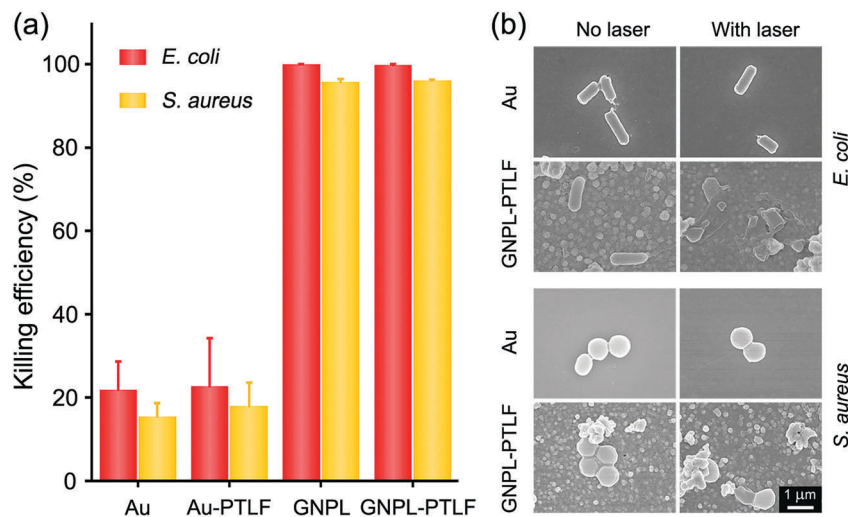


Fig. 4 Evaluation of the bactericidal activity of different surfaces with/without NIR laser irradiation ( $2.3 \text{ W cm}^{-2}$ , 5 min). (a) Photothermal bactericidal activity of surfaces against *E. coli* and *S. aureus* under NIR laser irradiation evaluated using a colony counting assay. Error bars represent the standard deviation of the mean ( $n = 3$ ). (b) Typical SEM images of attached bacteria on Au and GNPL-PTLF surfaces with/without NIR laser irradiation.

Au but caused serious damage to the outer membrane of bacteria on the GNPL-PTLF surface. It is suggested that the aggregates of GNPs convert absorbed NIR energy to heat sufficiently to cause denaturation of proteins and enzymes and irreversible damage to the membranes of bacteria, leading to destruction of bacterial activity and leakage of cellular contents.<sup>13–15,25,26</sup> This thermal killing mechanism has advantages including non-invasive nature, high efficiency, and non-generation of antibiotic resistance over traditional antibiotic-based approaches. Considering the data from these two different but complementary assays, it is concluded that GNPL-PTLF surfaces possess excellent broad-spectrum bactericidal activity under short-term NIR laser irradiation.

### 2.3. Triggered-release of killed bacteria

Similar to traditional antibacterial surfaces based on contact-killing mechanisms, most photothermal antibacterial surfaces suffer from the presence of killed bacteria which can provide nutrients for subsequent bacterial interactions, and trigger immune responses and/or inflammation. Therefore, it is of great interest to endow surfaces with bacteria-releasing properties so that bacteria are removed once they are killed, giving a renewed surface for long-term use. Previous smart antibacterial surfaces have taken advantage of surface-anchored stimuli-responsive polymers to switch surface functions between bacteria-killing and bacteria-releasing;<sup>36–42,59–62</sup> however, integration of these polymers usually involves multistep procedures that can only be used with specific substrates. In this work, we showed that PTLF was degraded in Vc solution. We thus hypothesized that after NIR treatment, the killed bacteria on the GNPL-PTLF surface would be removed along with the PTLF layer upon exposure to Vc solution. Because Vc treatment does not affect the GNPL, the “remaining” GNPL-PTLF surface should still exhibit photothermal bactericidal activity. This Vc-based bacteria-release function may provide a convenient and environmental-friendly solution to the residual dead bacteria problem.

The Vc-based bacteria-release capability of the GNPL-PTLF surface together with that of the control surfaces was therefore evaluated. After bacterial attachment and laser treatment as described above, the surfaces were gently rinsed to remove loosely bound bacteria and stained with a mixture of SYTO 9 (green fluorescent dye) and PI (red fluorescent dye) to label attached live and dead bacteria, respectively. The surfaces were then incubated in 100 mM Vc solution for 10 min and rinsed with buffer. The concentration of Vc and the incubation time were chosen based on preliminary data (Fig. S6 and S8, ESI<sup>†</sup>). The bacteria attached initially and remaining on the surfaces after Vc treatment were visualized and quantified using fluorescence microscopy. As shown in Fig. 5a, all of the bacteria on the GNPL-PTLF surface after laser treatment stained red, confirming the excellent bactericidal capability of this surface. Upon treatment with Vc solution, almost all of the bacteria were removed (Fig. 5b). The bacteria release ratios of the PTLF-containing surfaces (Au-PTLF and GNPL-PTLF) were >99%, whereas the surfaces without PTLF (Au and GNPL) showed negligible bacteria-releasing capability (release ratio <20%) (Fig. 5c and Fig. S9, ESI<sup>†</sup>), confirming that bacterial detachment was due to degradation of the PTLF. The degraded PTLF was easily washed away during the rinsing process leading to the possible loss of anchorage points for bacteria. Besides *E. coli* and *S. aureus*, we also tested the antibacterial performance of our GNPL-PTLF surface against a typical MDR bacterial strain, methicillin resistant *S. aureus* (MRSA). As shown in Fig. 6, the GNPL-PTLF surface also exhibited excellent photothermal bactericidal activity and Vc-induced bacterial release capability against MRSA, suggesting that the antibacterial performance is independent of the bacterial strains.

As mentioned above, the degradation of the PTLF takes place from the top layer and the extent of degradation is dependent on the concentration of Vc and the treatment time, suggesting that it is possible to “sequentially” degrade the PTLF by adjusting these two variables. These properties may thus be used as the

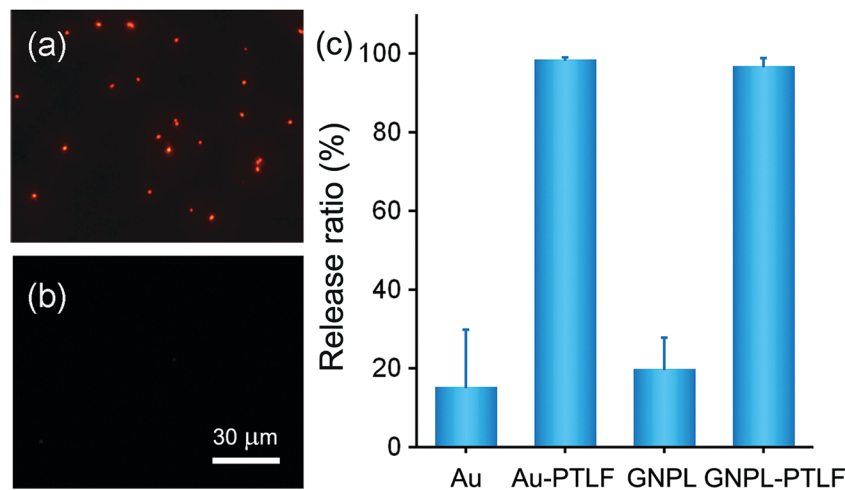


Fig. 5 (a and b) Representative fluorescence images of bacteria on the GNPL-PTLF surface after incubation in a suspension of *E. coli* at 37 °C: (a) before and (b) after incubation in 100 mM Vc solution for 10 min. (c) Bacterial release ratios of the different surfaces. Error bars represent standard deviation ( $n = 3$ ).

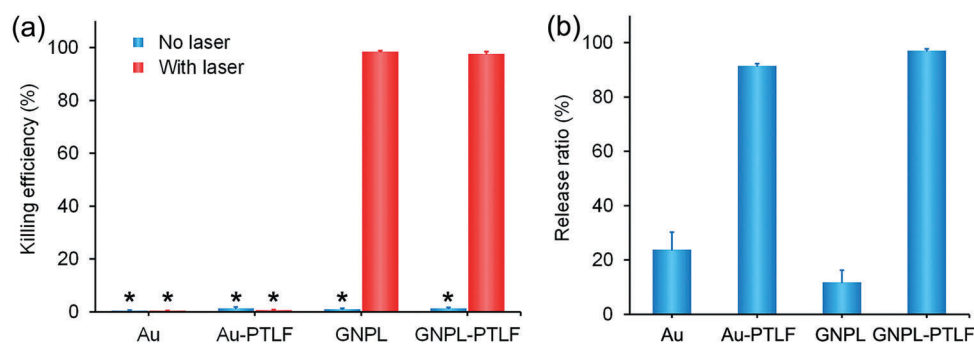


Fig. 6 (a) Photothermal bactericidal activity of different surfaces against methicillin resistant *S. aureus* (MRSA) under NIR laser irradiation ( $2.3 \text{ W cm}^{-2}$ , 5 min). (b) Vc-induced bacterial release ability of different surfaces. \* indicates killing efficiency < 2%. Error bars represent the standard deviation of the mean ( $n = 3$ ).

basis for a material that can undergo multiple cycles of “killing and release” of bacteria. To investigate this possibility, we prepared surfaces with thicker PTLFs using multiple coating

steps. These surfaces were treated sequentially with Vc solutions of increasing concentration for increasing times. It was found, for example, that the layer thickness on the Au-PTLF surface

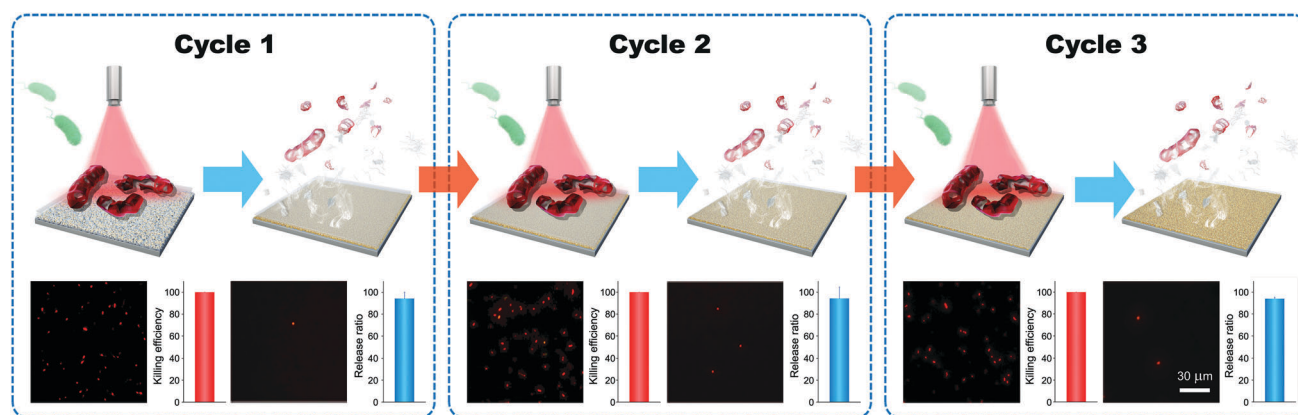


Fig. 7 Changes in antibacterial performance and properties of surfaces coated with a PTLF layer after sequential treatment with Vc of different concentrations and for different incubation times (50 mM Vc, 15 min for Cycle 1; 250 mM Vc, 30 min for Cycle 2; 500 mM Vc, 30 min for Cycle 3). Representative fluorescence images of bacteria on a GNPL-PTLF surface and the corresponding killing efficiency and release ratio over three “kill-release” cycles are shown. Error bars represent the standard deviation of the mean ( $n = 3$ ).

decreased from  $140.8 \pm 7.5$  nm to  $105.1 \pm 1.3$  nm after incubation with 50 mM Vc for 15 min, then to  $74.5 \pm 2.3$  nm after further incubation with 250 mM Vc for 30 min, and finally to  $30.1 \pm 3.1$  nm after further incubation with 500 mM Vc for 30 min (Fig. S10, ESI†). We then used a GNPL-PTLF surface with the same PTLF thickness to “challenge” *E. coli*. As shown in Fig. 7, in the first “kill-release” cycle, 99.9% of attached bacteria were killed and 94.3% were released by incubation with 50 mM Vc for 15 min, leaving a virtually clean GNPL-PTLF surface with a thinner PTLF. The same surface was then used in two additional “kill-release” cycles with Vc solution of higher concentration and longer incubation time. The GNPL-PTLF surface maintained high bactericidal activity and bacteria-release capability over three cycles, suggesting that (i) thicker PTLF did not influence the photothermal properties of the GNPL, and (ii) bacterial detachment was strongly correlated with the degradation of the topmost layer of PTLF. It is noted that both the bacteria-killing and bacteria-releasing processes were conducted in a simple and environmental-friendly manner, and the entire process for one “kill-release” cycle took less than 20 min.

#### 2.4. Storage stability and broad applicability

Stability is an important requirement for antibacterial surfaces. Antibacterial materials may become increasingly ineffective after continued exposure to air in storage or to physiological conditions in use. To investigate the storage stability and long-term effectiveness of our materials in complex biological medium, a set of GNPL-PTLF surfaces were prepared under identical conditions and then stored (in air or phosphate buffered saline (PBS, pH = 7.4)) or incubated (in human plasma or cell culture medium) up to 14 days. They were then tested for antibacterial performances against *E. coli*. It is found that after a 14 day storage in air or in PBS, the GNPL-PTLF surfaces retained their original bactericidal activity (>99% killing efficiency under NIR laser irradiation) and bacteria-release capability (>90% release ratio under Vc treatment). In addition, after a 14 day incubation in human plasma or cell culture medium, the GNPL-PTLF surfaces showed a slight decrease in bactericidal activity (but still >95% killing efficiency) and a relatively good bacteria-release capability (>70% release ratio) (Fig. S11 and S12, ESI†). Overall, these data indicate that the GNPL-PTLF surface remains stable over long times under appropriate storage conditions and exhibits long-term effectiveness when using this surface in actual application.

“Universality” is also important for any surface modification method, meaning that it should be applicable to diverse substrates having a range of surface chemistries and topographies.<sup>63–66</sup> For the present method, it has been demonstrated that both GNPL and PTLF can be deposited on various substrates *via* a facile chemical plating technique and a simple protein phase-transition process, respectively. It is thus expected that the GNPL-PTLF hybrid film may be applicable not only to model gold surfaces but to other more “practical” materials to endow them with antibacterial activity. To test the broad applicability of the method, several materials used in biomedical engineering applications including silicon (Si), polydimethylsiloxane (PDMS) and stainless steel (SS) were chosen as substrates to fabricate GNPL-PTLF

surfaces as described above. Successful preparation was confirmed by SEM and changes in the water contact angle during each modification step (Fig. S13 and Table S2, ESI†). The photothermal killing efficiency and bacterial releasing ability of these surfaces were evaluated using *E. coli*. As expected, all of the GNPL-PTLF surfaces exhibited strong bactericidal activity, killing >99.9% of attached bacteria on exposure to NIR laser irradiation. Moreover, the attached dead bacteria were easily removed from the surfaces by treatment with Vc (Fig. 8). Moreover, these GNPL-PTLF surfaces on different substrates also showed storage stability and long-term effectiveness as good as that on the model gold substrate

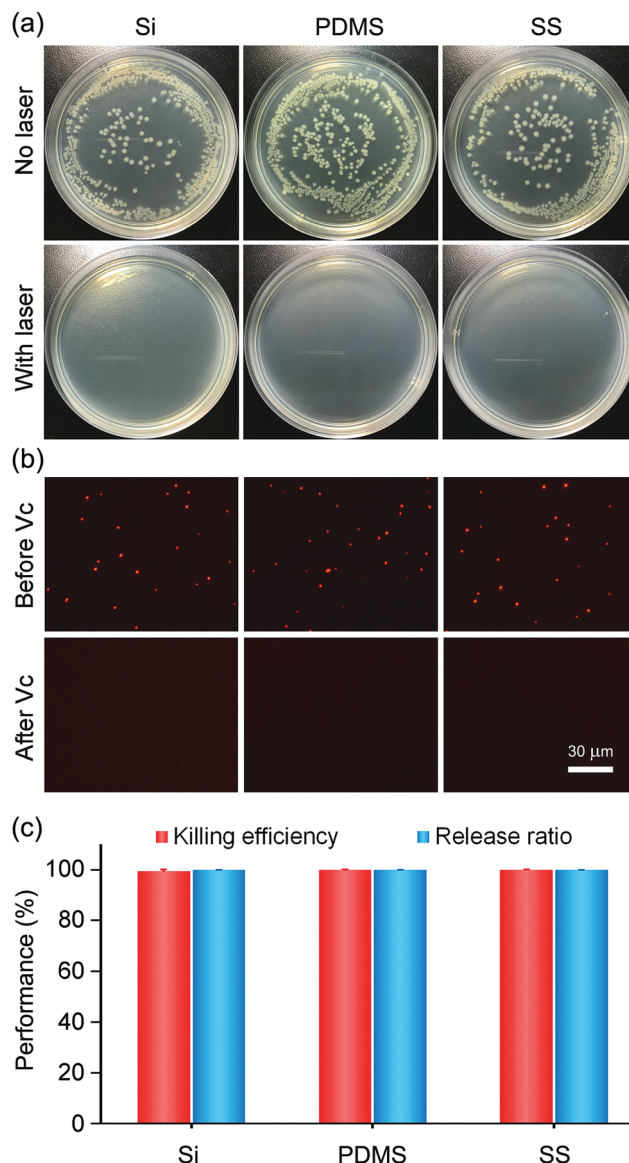


Fig. 8 (a) Typical photographs of *E. coli* colonies formed on agar plates after detachment from GNPL-PTLF surfaces with/without NIR laser irradiation on different substrates. (b) Representative fluorescence images of bacteria on GNPL-PTLF surfaces fabricated on various substrates before and after incubation in 100 mM Vc solution for 10 min. (c) The corresponding killing efficiency and release ratio of GNPL-PTLF surfaces fabricated on different substrates against *E. coli*. Error bars represent the standard deviation of the mean ( $n = 3$ ).

(Fig. S14–S16, ESI<sup>†</sup>). These data demonstrate that this surface modification method is applicable to diverse materials with different surface properties, and provide evidence of strong potential for its use in a range of practical applications.

### 3. Conclusion

In summary, we have developed a widely applicable strategy to endow surfaces with the capability to both kill attached bacteria efficiently and rapidly and remove dead bacteria and debris to maintain antibacterial properties over a long-term. This strategy involves the sequential deposition of a GNPL as a photothermal agent and PTLF as a “sacrificial” layer. A typical surface prepared on the gold substrate was able to kill >99% of attached bacteria under NIR laser irradiation for 5 min. In addition, subsequent incubation of the surface in Vc solution for 10 min removed the killed bacteria and regenerated bactericidal activity. The surface could be used and regenerated in this way through multiple cycles. It was also shown that the modified materials were stable over several days of storage in air or buffer. The method was applied to various substrate materials having a range of surface properties. These antibiotic-free, easily cleaned and regenerated hybrid films offer a viable alternative for the killing and removal of adherent bacteria (particularly multidrug resistant bacteria) on the surfaces of medical devices for *in vitro* applications.

### 4. Experimental section

#### Preparation of the gold nanoparticle layer (GNPL)

Preparation of the GNPL on substrates followed procedures reported previously.<sup>54</sup> In brief, the procedures for pretreatment of various substrates (Au, silicon, stainless steel (SS), poly(dimethylsiloxane) (PDMS)) to effect surface amination are described in the ESI<sup>†</sup>. The amino-functionalized surfaces were placed in the wells of 48-well plates after rinsing with ethanol several times and blow drying. After adjusting to pH  $\approx$  9 with 2 M NaOH, the plating solution (12 mM H<sub>2</sub>AuCl<sub>4</sub>·4H<sub>2</sub>O, 0.5 M KHCO<sub>3</sub>, and 25 mM glucose) at the desired volume was added to each well and maintained at 37 °C for 6 h to form the GNPL. The surfaces were removed from the solution, rinsed extensively with deionized water, and dried under a nitrogen stream.

#### Preparation of smooth substrates coated with PTLF and GNPL–PTLF

The fabrication of phase transitioned lysozyme films (PTLF) on the substrates followed the procedures reported previously.<sup>47</sup> The phase transition solution was freshly prepared by mixing lysozyme (2 mg mL<sup>-1</sup>) in stock buffer (10 mM HEPES buffer, pH 7.4) with TCEP buffer (50 mM TCEP in 10 mM HEPES buffer, pH 6.2) in a volume ratio of 1 : 1. Simple immersion is enough to transfer the PTLF efficiently onto the pristine surfaces (Au, Si, PDMS, SS) and the GNPL surfaces to form solid-supported nanofilms. Pristine or GNPL substrates were directly immersed in the freshly prepared phase transition solution, and after 2 h incubation, a conformal PTLF was stably attached. The coated

materials were then rinsed with fresh HEPES buffer to remove lysozyme and buffer salts. The coated materials were investigated after vacuum drying.

#### Surface characterization

Water contact angles and layer thicknesses were measured at room temperature using an SL200C optical contact angle meter (Solon Information Technology Co., Ltd) and an M-88 spectroscopic ellipsometer (J. A. Woollam Co., Inc.), respectively. Six replicates were measured for each surface type. Surface elemental composition was determined using X-ray photoelectron spectroscopy (XPS, UK VG Scientific Ltd), and surface morphology was observed using scanning electron microscopy (SEM, S-4700, Hitachi).

#### Photothermal properties of the surfaces

Continuous-wave laser light with a wavelength of 808 nm was used throughout. To measure the photothermal properties of the surfaces, completely dry samples were exposed to NIR laser light at a power density of 2.3 W cm<sup>-2</sup>, and the surface temperature was recorded using an infrared thermal camera (Infrared Cameras. Inc.).

#### Degradation of PTLF with Vc solution

Degradation of PTLF was evaluated in Vc solutions of different concentration (50, 100, 200 and 500 mM) for different times (5, 10, 15 and 20 min). The water contact angles and layer thicknesses of the surfaces before and after degradation were measured using an SL200C optical contact angle meter (Solon Information Technology Co., Ltd) and an atomic force microscope (AFM) equipped with a multimode Nanoscope V scanning probe microscopy system (Bruker Co., Ltd, USA), respectively. The elemental compositions of GNPL and GNPL–PTLF surfaces before and after Vc treatment were determined using X-ray photoelectron spectroscopy (XPS, UK VG Scientific Ltd).

#### Biocidal activity assays

Briefly, samples were placed in the wells of a 48-well plate, with the test surface facing up, and incubated in 500  $\mu$ L of the bacterial suspension at 37 °C for 1 h without stirring. They were then gently rinsed with sterile water to remove loosely attached cells and buffer salts. The samples were then placed in 250  $\mu$ L PBS and exposed to laser irradiation at a power density of 2.3 W cm<sup>-2</sup> for a specified time. The biocidal activity of the samples was assessed using *E. coli* ( $1 \times 10^7$  cells mL<sup>-1</sup> in PBS, pH = 7.4) and *S. aureus*/MRSA suspensions ( $1 \times 10^7$  cells mL<sup>-1</sup> in PBS, pH = 7.4) via live/dead staining assay, scanning electron microscopy (SEM), and colony counting assay (see details in ESI<sup>†</sup>).

#### Attachment and detachment of bacteria

The attachment and detachment of bacteria were assessed using an *E. coli* suspension ( $1 \times 10^7$  cells mL<sup>-1</sup> in PBS, pH = 7.4). In brief, the samples were incubated in 500  $\mu$ L of the suspension at 37 °C for 1 h without stirring and then irradiated. They were then gently rinsed with sterile water to remove loosely attached cells and buffer salts. For bacterial detachment, the surfaces with adherent bacteria were immersed in a sterile Vc solution for a specified time

and then rinsed with sterile water. The staining assay was then carried out as described in ESL.† The number of bacteria remaining attached on the surfaces was determined using a fluorescence microscope (IX71, Olympus, Japan) with a 40× objective, and the images of 15 randomly chosen fields were captured. Three replicates were examined, and the density of adherent bacteria was determined using Image-Pro Plus software.

## Conflicts of interest

There are no conflicts to declare.

## Acknowledgements

This work was supported by the National Key Research and Development Program of China (2016YFC1100402), the National Natural Science Foundation of China (21774086, 21334004, 51673112 and 21374057), the China Postdoctoral Science Foundation (2017M623109), and the Priority Academic Program Development of Jiangsu Higher Education Institutions (PAPD). The authors thank Prof. John Brash for helpful discussions.

## References

- L. Hall-Stoodley, J. W. Costerton and P. Stoodley, *Nat. Rev. Microbiol.*, 2004, **2**, 95–108.
- M. Katsikogianni and Y. F. Missirlis, *Eur. Cells Mater.*, 2004, **8**, 37–57.
- S. Y. Tan, S. C. Chew, M. Givskov and L. Yang, *Curr. Opin. Biotechnol.*, 2014, **26**, 1–6.
- N. Hadjesfandiari, K. Yu, Y. Mei and J. N. Kizhakkedathu, *J. Mater. Chem. B*, 2014, **2**, 4968–4978.
- M. Cloutier, D. Mantovani and F. Rosei, *Trends Biotechnol.*, 2015, **33**, 637–652.
- A. Jain, L. S. Duvvuri, S. Farah, N. Beyth, A. J. Domb and W. Khan, *Adv. Healthcare Mater.*, 2014, **3**, 1969–1985.
- G. A. Junter, P. Thebault and L. Lebrun, *Acta Biomater.*, 2016, **30**, 13–25.
- L. Rizzello and P. P. Pompa, *Chem. Soc. Rev.*, 2014, **43**, 1501–1518.
- A. Kugel, S. Stafslin and B. J. Chisholm, *Prog. Org. Coat.*, 2011, **72**, 222–252.
- C. C. Fuglsang, C. Johansen, S. Christgau and J. Adler-Nissen, *Trends Food Sci. Technol.*, 1995, **6**, 390–396.
- M. Bassetti, M. Merelli, C. Temperoni and A. Astilean, *Ann. Clin. Microbiol. Antimicrob.*, 2013, **12**, 22.
- M. F. Chellat, L. Raguž and R. Riedl, *Angew. Chem., Int. Ed.*, 2016, **55**, 6600–6626.
- M. Wilson, *J. Appl. Bacteriol.*, 1993, **75**, 299–306.
- P. C. Ray, S. A. Khan, A. K. Singh, D. Senapati and Z. Fan, *Chem. Soc. Rev.*, 2012, **41**, 3193–3209.
- Y. Shi, M. Liu, F. Deng, G. Zeng, Q. Wan, X. Zhang and Y. Wei, *J. Mater. Chem. B*, 2017, **5**, 194–206.
- Y. Yang, J. Aw and B. Xing, *Nanoscale*, 2017, **9**, 3698–3718.
- K. C. Black, T. S. Sileika, J. Yi, R. Zhang, J. G. Rivera and P. B. Messersmith, *Small*, 2014, **10**, 169–178.
- Y. Zhu, M. Ramasamy and D. K. Yi, *ACS Appl. Mater. Interfaces*, 2014, **6**, 15078–15085.
- D. G. Meeker, S. V. Jenkins, E. K. Miller, K. E. Beenken, A. J. Loughran, A. Powless, T. J. Muldoon, E. I. Galanzha, V. P. Zharov, M. S. Smeltzer and J. Chen, *ACS Infect. Dis.*, 2016, **2**, 241–250.
- C. P. Teng, T. Zhou, E. Ye, S. Liu, L. D. Koh, M. Low, X. J. Loh, K. Y. Win, L. Zhang and M. Y. Han, *Adv. Healthcare Mater.*, 2016, **5**, 2122–2130.
- M.-C. Wu, A. R. Deokar, J.-H. Liao, P.-Y. Shih and Y.-C. Ling, *ACS Nano*, 2013, **7**, 1281–1290.
- D. Lin, T. Qin, Y. Wang, X. Sun and L. Chen, *ACS Appl. Mater. Interfaces*, 2014, **6**, 1320–1329.
- X. Yang, Z. Li, E. Ju, J. Ren and X. Qu, *Chem. – Eur. J.*, 2014, **20**, 394–398.
- E. Ju, Z. Li, M. Li, K. Dong, J. Ren and X. Qu, *Chem. Commun.*, 2013, **49**, 9048–9050.
- A. Gharatape, S. Davaran, R. Salehi and H. Hamishehkar, *RSC Adv.*, 2016, **6**, 111482–111516.
- A. Bucharskaya, G. Maslyakova, G. Terentyuk, A. Yakunin, Y. Avetisyan, O. Bibikova, E. Tuchina, B. Khlebtsov, N. Khlebtsov and V. Tuchin, *Int. J. Mol. Sci.*, 2016, **17**, 1295.
- N. J. Millenbaugh, J. B. Baskin, M. N. DeSilva, W. R. Elliott and R. D. Glickman, *Int. J. Nanomed.*, 2015, **10**, 1953–1960.
- R. S. Norman, J. W. Stone, A. Gole, C. J. Murphy and T. L. Sabo-Attwood, *Nano Lett.*, 2008, **8**, 302–306.
- D. Hu, H. Li, B. Wang, Z. Ye, W. Lei, F. Jia, Q. Jin, K.-F. Ren and J. Ji, *ACS Nano*, 2017, **11**, 9330–9339.
- S. H. Kim, E. B. Kang, C. J. Jeong, S. M. Sharker, I. In and S. Y. Park, *ACS Appl. Mater. Interfaces*, 2015, **7**, 15600–15606.
- W. Lei, K. Ren, T. Chen, X. Chen, B. Li, H. Chang and J. Ji, *Adv. Mater. Interfaces*, 2016, **3**, 1600767.
- Y. K. Kim, E. B. Kang, S. M. Kim, C. P. Park, I. In and S. Y. Park, *ACS Appl. Mater. Interfaces*, 2012, **9**, 3192–3200.
- L. Mi and S. Jiang, *Angew. Chem., Int. Ed.*, 2014, **53**, 1746–1754.
- Q. Yu, Z. Wu and H. Chen, *Acta Biomater.*, 2015, **16**, 1–13.
- T. Wei, Z. Tang, Q. Yu and H. Chen, *ACS Appl. Mater. Interfaces*, 2017, **9**, 37511–37523.
- Z. Cao, L. Mi, J. Mendiola, J. R. Ella-Menye, L. Zhang, H. Xue and S. Jiang, *Angew. Chem., Int. Ed.*, 2012, **51**, 2602–2605.
- Q. Yu, J. Cho, P. Shivapooja, L. K. Ista and G. P. Lopez, *ACS Appl. Mater. Interfaces*, 2013, **5**, 9295–9304.
- Q. Yu, W. Ge, A. Atewologun, A. D. Stiff-Roberts and G. P. Lopez, *J. Mater. Chem. B*, 2014, **2**, 4371–4378.
- Q. Yu, W. Ge, A. Atewologun, A. D. Stiff-Roberts and G. P. Lopez, *Colloids Surf., B*, 2015, **126**, 328–334.
- S. Yan, H. Shi, L. Song, X. Wang, L. Liu, S. Luan, Y. Yang and J. Yin, *ACS Appl. Mater. Interfaces*, 2016, **8**, 24471–24481.
- Z. Q. Shi, Y. T. Cai, J. Deng, W. F. Zhao and C. S. Zhao, *ACS Appl. Mater. Interfaces*, 2016, **8**, 23523–23532.
- T. Wei, W. Zhan, Q. Yu and H. Chen, *ACS Appl. Mater. Interfaces*, 2017, **9**, 25767–25774.
- C. Burda, X. Chen, R. Narayanan and M. A. El-Sayed, *Chem. Rev.*, 2005, **105**, 1025–1102.
- Z. Lyu, F. Zhou, Q. Liu, H. Xue, Q. Yu and H. Chen, *Adv. Funct. Mater.*, 2016, **26**, 5787–5795.

- 45 J. Wu, H. Xue, Z. Lyu, Z. Li, Y. Qu, Y. Xu, L. Wang, Q. Yu and H. Chen, *ACS Appl. Mater. Interfaces*, 2017, **9**, 21593–21598.
- 46 Y. Ha, J. Yang, F. Tao, Q. Wu, Y. Song, H. Wang, X. Zhang and P. Yang, *Adv. Funct. Mater.*, 2018, **28**, 1704476.
- 47 J. Gu, Y. Su, P. Liu, P. Li and P. Yang, *ACS Appl. Mater. Interfaces*, 2017, **9**, 198–210.
- 48 P. Yang, *Macromol. Biosci.*, 2012, **12**, 1053–1059.
- 49 Z. Wu and P. Yang, *Adv. Mater. Interfaces*, 2015, **2**, 1400401.
- 50 A. Gao, Q. Wu, D. Wang, Y. Ha, Z. Chen and P. Yang, *Adv. Mater.*, 2016, **28**, 579–587.
- 51 F. Tao, Q. Han, K. Liu and P. Yang, *Angew. Chem., Int. Ed.*, 2017, **56**, 13440–13444.
- 52 D. Wang, Y. Ha, J. Gu, Q. Li, L. Zhang and P. Yang, *Adv. Mater.*, 2016, **28**, 7414–7423.
- 53 J. Gu, S. Miao, Z. Yan and P. Yang, *Colloid Interface Sci. Commun.*, 2018, **22**, 42–48.
- 54 F. Zhou, L. Yuan, H. Wang, D. Li and H. Chen, *Langmuir*, 2011, **27**, 2155–2158.
- 55 S. Wang, K. Liu, X. Yao and L. Jiang, *Chem. Rev.*, 2015, **115**, 8230–8293.
- 56 S. Eustis and M. A. El-Sayed, *Chem. Soc. Rev.*, 2006, **35**, 209–217.
- 57 W. Lee, I. Kim, S. W. Lee, H. Lee, G. Lee, S. Kim, S. W. Lee and D. S. Yoon, *Macromol. Res.*, 2016, **24**, 868–873.
- 58 J. Kennedy, I. S. Blair, D. A. McDowell and D. J. Bolton, *J. Appl. Microbiol.*, 2005, **99**, 1229–1235.
- 59 B. Wang, Q. Xu, Z. Ye, H. Liu, Q. Lin, K. Nan, Y. Li, Y. Wang, L. Qi and H. Chen, *ACS Appl. Mater. Interfaces*, 2016, **8**, 27207–27217.
- 60 T. Wei, Q. Yu, W. Zhan and H. Chen, *Adv. Healthcare Mater.*, 2016, **5**, 449–456.
- 61 B. Wu, L. Zhang, L. Huang, S. Xiao, Y. Yang, M. Zhong and J. Yang, *Langmuir*, 2017, **33**, 7160–7168.
- 62 Q. Yu, L. K. Ista and G. P. Lopez, *Nanoscale*, 2014, **6**, 4750–4757.
- 63 H. Lee, Y. Lee, A. R. Statz, J. Rho, T. G. Park and P. B. Messersmith, *Adv. Mater.*, 2008, **20**, 1619–1623.
- 64 Q. Wei and R. Haag, *Mater. Horiz.*, 2015, **2**, 567–577.
- 65 L. Cao, Y. Qu, C. Hu, T. Wei, W. Zhan, Q. Yu and H. Chen, *Adv. Mater. Interfaces*, 2016, **3**, 1600600.
- 66 T. Wei, W. Zhan, L. Cao, C. Hu, Y. Qu, Q. Yu and H. Chen, *ACS Appl. Mater. Interfaces*, 2016, **8**, 30048–30057.